PHYSICAL REVIEW D **96,** 022002 (2017)

Brownian thermal noise in functional optical surfaces

S. Kroker*
Physikalisch-Technische Bundesanstalt, Bundesallee 100, 38116 Braunschweig, Germany and Technische Universität Braunschweig, LENA Laboratory for Emerging Nanometrology, Pockelsstraße 14, 38106 Braunschweig, Germany

J. Dickmann and C. B. Rojas Hurtado
Physikalisch-Technische Bundesanstalt, Bundesallee 100, 38116 Braunschweig, Germany

D. Heinert and R. Nawrodt
Friedrich-Schiller-Universität Jena, Institut für Festkörperphysik, Helmholtzweg 5, 07743 Jena, Germany

Y. Levin
School of Physics and Astronomy, Monash University, P.O. Box 27, VIC 3800, Australia

S. P. Vyatchanin
Faculty of Physics, Moscow State University, Moscow 119991, Russia
(Received 29 April 2017; published 10 July 2017)

We present a formalism to compute Brownian thermal noise in functional optical surfaces such as grating reflectors, photonic crystal slabs, or complex metamaterials. Such computations are based on a specific readout variable, typically a surface integral of a dielectric interface displacement weighed by a form factor. This paper shows how to relate this form factor to Maxwell's stress tensor computed on all interfaces of the moving surface. As an example, we examine Brownian thermal noise in monolithic T-shaped grating reflectors. The previous computations by Heinert *et al.* [Phys. Rev. D **88**, 042001 (2013)] utilizing a simplified readout form factor produced estimates of thermal noise that are tens of percent higher than those of the exact analysis in the present paper. The relation between the form factor and Maxwell's stress tensor implies a close correlation between the optical properties of functional optical surfaces and thermal noise.

DOI: 10.1103/PhysRevD.96.022002

I. INTRODUCTION

Thermal noise sets a crucial limitation to several high-precision instruments, for example, ultrastable laser resonators for the realization of optical clocks, high resolution optical spectroscopy, and gravitational wave detectors [1–6]. Particularly, Brownian displacement noise from random motion of amorphous optical coatings, as utilized for high-reflectivity Bragg mirrors, represents a severe bottleneck for future sensitivity improvements of these measurement systems [7–11]. The reason for the large Brownian noise amplitude is the high mechanical loss of the coating materials. Currently, several approaches to reduce Brownian coating thermal noise are under investigation, for example, optimizing the mechanical properties of amorphous materials, or using crystalline coating stacks based on AlGaAs/GaAs and AlGaP/GaP as low-loss coating materials [12–17].

As an alternative to Bragg mirrors, grating reflectors based on crystalline silicon have been theoretically proposed [18] and experimentally realized [19–21]. Since these elements can be monolithically implemented without adding any amorphous material with high mechanical loss, they are promising as low-noise optical components. In contrast to Bragg mirrors, in grating reflectors high reflectivity is realized by an optical resonance which leads to a penetration of the light into a surface layer with a thickness of only a few hundred nanometers [22,23]. Figure 1 illustrates a typical field distribution in a monolithic high-reflectivity structure. The lower grating region acts as a supporting structure that prevents the light from leaking into the substrate.

A typical task in high-precision optomechanical experiments is to measure the phase shift of light reflected from a mirror surface or, alternatively, the change of the optical mode frequency if the mirror is a part of the optical resonator. For small displacements, this readout variable depends linearly on the displacement of the reflecting surface. It can be expressed as

$$\hat{z}(t) = \int f(\vec{r}) u_{\perp}(\vec{r}, t) \mathrm{d}A. \tag{1}$$

$\vec{r}$ is the location of a point on the surface, and $u_{\perp}(\vec{r}, t)$ is the displacement of the mirror perpendicular to the surface A at $\vec{r}$ and time t. The form factor $f(\vec{r})$ depends on the intensity profile of the laser beam and is proportional to the laser

*stefanie.kroker@ptb.de

light intensity at $\vec{r}$ as will be shown below. In the case of a planar surface the form factor is simply the laser beam profile, whereas in the case of a structured surface the determination of $f(\vec{r})$ is a nontrivial task. The standard way to compute thermal noise in this variable is to use a formulation of the fluctuation-dissipation theorem by Callen and Welton [24] which employs a virtual oscillating pressure of the form [7]

$$p(\vec{r}) = F_0 \cos(\omega t) f(\vec{r}), \tag{2}$$

where F_0 is an arbitrary constant characterizing the total force applied to the surface and $f(\vec{r})$ is the form factor of Eq. (1). The virtual pressure is utilized to determine the strain energy density $\epsilon(x, y, z)$. This strain distribution then serves as a basis to calculate the dissipated mechanical energy in the system at a given frequency ω. Using the model of structural loss, the dissipated energy reads [7]

$$W_{\mathrm{diss}}(\omega) = \omega \int \epsilon(\vec{r}) \phi(\vec{r}) \mathrm{d}V, \tag{3}$$

with $\phi(\vec{r})$ as the mechanical loss angle. The integral in Eq. (3) needs to be performed over the whole component under investigation. The Brownian thermal noise power spectral density can be expressed by

$$S_z(\omega, T) = \frac{8 k_B T}{\omega^2} \frac{W_{\mathrm{diss}}}{F_0^2}. \tag{4}$$

The challenge is to compute the form factor on arbitrary surfaces, and this paper gives a direct and exact answer. The previous approach by Heinert *et al.* [25] gave an approximation by assuming that the form factor was constant on large segments on the interface. Heinert *et al.* evaluated the impact on the overall phase shift of the reflected light by displacing these segments as a whole. In contrast, this paper finds that the form factor is strongly inhomogeneous, which significantly affects the computation of thermal noise spectral density.

As an application of our formalism, we investigate Brownian thermal noise in monolithic silicon T-shaped grating reflectors and compare the results with the work by Heinert *et al.* [25]. In addition, we investigate the impact of width of the support structure as a critical parameter for Brownian thermal noise. We find that an optimum support structure width exists which minimizes Brownian noise. Due to manufacturing errors, the geometric dimensions of the grating may differ from the design values by a few nanometers. We evaluate the consequences of manufacturing errors and show that it may lead to deviations of thermal noise by a factor of about 2.5.

The article is organized as follows: In Sec. II we introduce the calculation method based on Maxwell's stress tensor. In Sec. III we discuss the components of Maxwell's stress tensor in T-shape grating reflectors. Afterwards, in Sec. IV we explain how the geometric grating parameters of T-shaped grating reflectors with different support structure widths were defined. In Sec. V we utilize these parameters to compute the virtual forces required for the thermal noise calculations, the energy of elastic deformation in response to these forces, and finally the Brownian thermal noise.

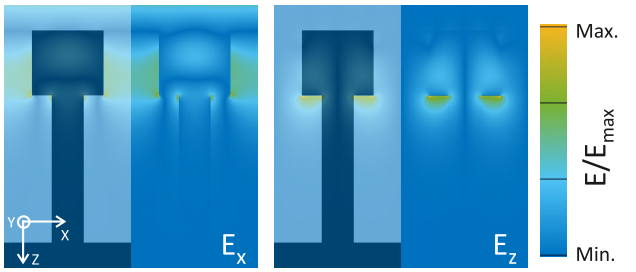

FIG. 1. Distribution of E_x and E_z in the high-reflectivity grating reflector discussed by Heinert *et al.* [25]. The calculation was performed by means of the rigorous coupled wave analysis (RCWA) [26] for a wavelength of 1550 nm, normal incidence and transverse-magnetic polarized light.

II. CALCULATION OF BROWNIAN THERMAL NOISE IN FUNCTIONAL OPTICAL SURFACES

The form factor can be described following [27,28]. Let us first consider an optical cavity of length L. When one of the two mirrors is moved by a displacement of z, the eigenfrequency ω of the cavity is changed by $\delta\omega$:

$$\frac{\delta\omega}{\omega} = \frac{z}{L}. \tag{5}$$

The quantity z contains the measurement signal, e.g., a gravitational wave signal. But also random perturbations $u_\perp(\vec{r})$ caused by Brownian motion may contribute to a frequency change and thus disturb the measurement signal. The question to be answered is how such a displacement translates into the frequency change of the cavity. A slow displacement does not change the number of photons in the cavity. This condition of adiabaticity is satisfied very well if the frequencies of interest are much smaller than the inverse light round trip inside the cavity, as is valid for the LIGO gravitational wave detector. In this case the relation

$$\frac{\mathcal{E}}{\omega} = \mathrm{const.} \tag{6}$$

is fulfilled, where $\mathcal{E}$ represents the energy of the eigenmode. Therefore, a change of the energy $\delta\mathcal{E}$ may be converted into a frequency change of the optical eigenmode:

$$\frac{\delta\mathcal{E}}{\mathcal{E}} = \frac{\delta\omega}{\omega}. \tag{7}$$

The energy change is a result of the work performed against the ponderomotive pressure perpendicular to the surface $p_\perp$.

Thus, the energy change of the optical cavity mode caused by displacements $u_\perp(\vec{r})$ can be expressed by

$$\delta\mathcal{E} = \int p_\perp(\vec{r}) u_\perp(\vec{r}) \mathrm{d}A. \tag{8}$$

The ponderomotive pressure relates a perturbation $u_\perp(\vec{r})$ of an arbitrary surface to an effective translation $\hat{u}$ of the cavity mirror as a whole:

$$\hat{z} = \frac{L}{\mathcal{E}} \int p_\perp(\vec{r}) u_\perp(\vec{r}) \mathrm{d}A. \tag{9}$$

The ponderomotive light pressure results from the difference of Maxwell's stress tensor on both sides of the interface:

$$p_\perp(\vec{r}) = \Delta\sigma_{ij}(\vec{r}) n_i n_j, \tag{10}$$

where n_i is the unit vector normal to the surface and a summation over the dummy indices i and j is implied. Maxwell's stress tensor with SI units reads

$$\sigma_{ij} = \varepsilon_0 \varepsilon_\mathrm{r} E_i E_j + \frac{1}{\mu_0 \mu_\mathrm{r}} B_i B_j - \frac{1}{2}\left(\varepsilon_0 \varepsilon_\mathrm{r} E^2 + \frac{1}{\mu_0 \mu_\mathrm{r}} B^2\right)\delta_{ij}. \tag{11}$$

ε_0 and μ_0 are the dielectric and magnetic field constants, E_i is the vacuum electric field amplitude, and B_i is the magnetic field amplitude, respectively. On arbitrary surfaces, the electromagnetic field distribution can be calculated with the finite element tool COMSOL [29]. In the following sections, we will use the Maxwell stress tensor to evaluate the virtual forces in T-shaped monolithic grating reflectors and derive the Brownian thermal noise thereof. Since the electric and magnetic fields depend on the position at the surface, the stress tensor components σ_{ij} are also a function of the position. For the sake of readability, we will omit this explicit spatial dependency in our notation.

III. VIRTUAL PRESSURE IN MONOLITHIC T-SHAPED GRATING REFLECTORS

In a T-shaped structure the relevant components of the stress tensor are σ_{xx} and σ_{zz} (see Fig. 2) and the resulting pressure is the difference of the pressures inside and outside the structure. For nonmagnetic materials ($\mu_\mathrm{r} = 1$) the relevant pressure components at the grating surface are

$$\Delta\sigma_{xx} = \frac{\varepsilon_0}{2}(\varepsilon_\mathrm{r} - 1)\left(\frac{E_\mathrm{x}^2}{\varepsilon_\mathrm{r}} + E_\mathrm{y}^2 + E_\mathrm{z}^2\right), \tag{12}$$

$$\Delta\sigma_{zz} = \frac{\varepsilon_0}{2}(\varepsilon_\mathrm{r} - 1)\left(\frac{E_\mathrm{z}^2}{\varepsilon_\mathrm{r}} + E_\mathrm{y}^2 + E_\mathrm{x}^2\right). \tag{13}$$

where E_x, E_y, and E_z are the vacuum fields and ε_r is the relative permittivity of the grating material. To relate our method to the results of Heinert *et al.* [25], we will restrict our considerations on light with transverse magnetic (TM) polarization ($E_y = 0$). In this case the pressure components reduce to

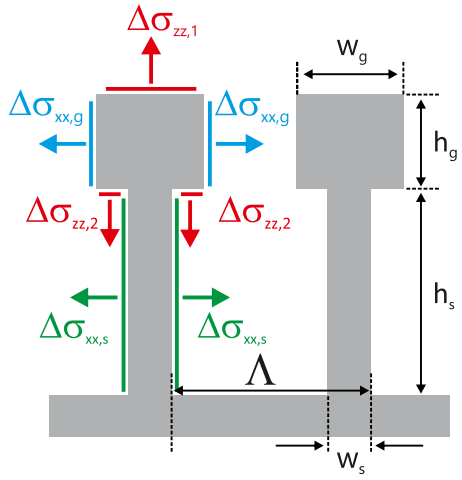

FIG. 2. Distribution of the virtual pressure components (left). Overview of the geometric structure parameters (right).

$$\Delta\sigma_{xx} = \frac{\varepsilon_0}{2}(\varepsilon_\mathrm{r} - 1)\left(\frac{E_\mathrm{x}^2}{\varepsilon_\mathrm{r}} + E_\mathrm{z}^2\right), \tag{14}$$

$$\Delta\sigma_{zz} = \frac{\varepsilon_0}{2}(\varepsilon_\mathrm{r} - 1)\left(\frac{E_\mathrm{z}^2}{\varepsilon_\mathrm{r}} + E_\mathrm{x}^2\right). \tag{15}$$

By using finite element analysis, the pressure components can be calculated and applied to the surface of the structure [29]. Using Eq. (9), one can show that F_0 is the overall radiation pressure force from the light beam onto the mirror. One can evaluate it directly from the Maxwell stresses at the dielectric interface. In this case one should carefully keep track of the sign contributions from the force applied at different segments of the grating as shown in Fig. 2. The resulting force F_0 is the integral of the pressure over the surface A of a single period normalized to a unity length in the y-direction parallel to the ridges. The elastic energy then is the volume integral of the energy density ϵ over one T-shaped ridge. In combination with the mechanical loss $\phi(x, y, z)$, this yields the dissipated energy W_diss [see Eq. (3)]. In the 1D periodic structure three main contributions may be identified: the elastic energy due to the $\pm\sigma_{zz}$ pressures on the front and back side of the optical grating (i.e., the upper grating region); the elastic energy due to the $\pm\sigma_{xx}$ pressures on the side walls of the optical grating; and the elastic energy caused by the $\pm\sigma_{xx}$ pressures on the side walls of the supporting structure. Cross terms account for about 5% of the total elastic energy. The field distribution in the structure and thereby the stress tensor component depend on the geometric parameters of the grating structure. Thus, before calculating thermal noise

in the structure, in the following section we will explain how suitable parameters yielding high reflectivity are determined.

IV. CHOICE OF GEOMETRIC GRATING PARAMETERS

As shown in Fig. 2, five parameters characterize the structure of a grating reflector: grating period Λ, width w_g, and depth h_g of the optical grating, as well as width w_s and depth h_s of the support structure. We utilize the rigorous coupled wave analysis (RCWA) [26], a standard tool to solve Maxwell's equations in periodic structures, for the computation of reflectivity and to explore how the reflectivity depends on the grating parameters. The basic requirements for suitable parameter sets are high reflectivity, low field enhancement inside the structure to minimize virtual pressure, and possibly compact structures to minimize the elastic deformation energy. Thus, we choose high-reflectivity configurations employing low-Q optical resonances with low field enhancement [23] and minimize the total depth $h_g + h_s$. As mentioned above, the supporting structure's task is to optically decouple the optical grating from the substrate. The penetration depth of light into the support increases with decreasing refractive index contrast between the optical grating and the support structure. The index contrast, in turn, is determined by the width w_s of the supporting structure. Hence w_s is an important parameter for Brownian thermal noise and is used as a free parameter in the following discussions.

For a given w_s, the size of the parameter space $\{w_g, h_g\}$ providing high reflectivity depends on the grating period Λ. Its shape and position is determined by the complex interplay of two Bloch modes propagating in the optical grating. This mechanism for high reflectivity is discussed in detail in the works by Lalanne *et al.* [22] and Karagodsky *et al.* [30]. Figure 3 illustrates the range $\{w_g, h_g\}$ calculated with RCWA for three different periods. In order to achieve large fabrication tolerances, the high-reflectivity range of w_g and h_g has to be maximized. As illustrated in Fig. 3, the size of the relevant parameter range grows with increasing grating period. However, for large grating periods the high-reflectivity domain in the $w_g - h_g$ plain degenerates to a

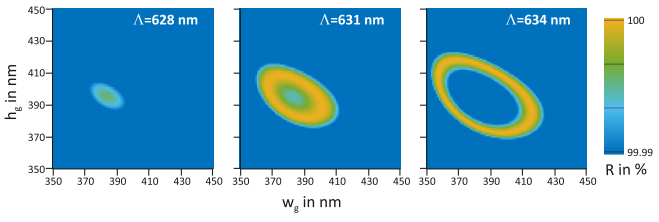

FIG. 3. Calculated high-reflectivity parameter range $\{w_g, h_g\}$ for different periods. A supporting structure width w_s of 40 nm was utilized. The incident light has a wavelength of 1550 nm, an incidence angle of 0° and transverse-magnetic polarization.

TABLE I. Structure parameters for $R > 99.99\%$. In the h_g-w_g plot (see Fig. 3) the parameter sets represent the center of the highly reflective parameter space $\{w_g, h_g\}$ for a wavelength of 1550 nm, normal incidence, and TM polarization. Additionally, the structure parameters utilized by Heinert *et al.* [25] are displayed.

w_s (nm)	Λ (nm)	h_s (nm)	w_g (nm)	h_g (nm)
40	631	640	385	395
60	633	630	385	392
80	637	620	382	390
100	642	620	384	384
120	649	630	384	379
140	660	670	386	371
160	675	750	385	361
172[a]	688	800	388	350
180	701	920	391	345
200	739	1280	397	335
220	776	2200	409	322

[a]Structure used by Heinert *et al.* [25].

ring which is detrimental in terms of fabrication tolerances if the reflectivity drops below the target value inside the enclosed area. For each target reflectivity R, which is typically $R \geq 99.99\%$ [31], there exists an optimal period which maximizes the size of the simply connected high-reflectivity area. With $R \geq 99.99\%$, the optimal period for the configuration investigated in Fig. 3 is 631 nm. The optimal working point is then located in the center of the area obeying $R \geq 99.99\%$. The depth of the supporting structure h_s does not substantially influence the reflectivity distribution within the parameter range $\{w_g, h_g\}$. To achieve structures that are as compact as possible, at the end of the optimization process the minimal h_s for $R \geq 99.99\%$ may be chosen. Following this strategy, the optimal parameters in dependence of support structure widths w_s were determined. The resulting values are shown in Table I. It is noteworthy that enhancing w_s from 40 nm to 220 nm increases h_s by a factor of 3.4, whereas the other parameters change by less than 20%.

V. RESULTS AND DISCUSSION

With the grating parameters shown in Table I, the stress tensor, the pressure, and the resulting force F_0 at the grating surface were calculated. The computation of the elastic stress distribution within the grating structure was performed with the finite element tool COMSOL [29]. All calculations refer to an incident light power of 1 W. The power determines the absolute values of the forces and of the elastic energy but it has no influence on the thermal noise amplitude [27,28]. The related material parameters are illustrated in Table II. Figure 4 shows the contributions of the different interfaces to the total force. The colors of the data points correspond to the colors used in Fig. 2. For small w_s the force at the back side of the optical grating

TABLE II. Material parameters for silicon. ϕ_{grat} is the mechanical loss of the grating structure, ρ the density, Y the Young's modulus, and σ the Poisson ratio.

	$T = 300$ K	$T = 10$ K
ϕ_{grat}	5×10^{-5} [32]	1×10^{-5} [33]
ρ in kg/m^3	2331	
Y in GPa	130 [34]	
σ	0.28 [34]	

dominates the contributions from the other interfaces. A very similar situation was found by Heinert *et al.* [25]. There, the magnitude of the force at the front side is by a factor of 54 smaller than the force at the back side. Our calculations reveal a factor of 57. The dominance of the forces at the back side are a consequence of the E_z distribution in the structure (see Fig. 1), which is enhanced at the back side of the optical grating.

In the x-direction, for small w_s the optical grating contributes more to the force than the support structure, because the electromagnetic field barely penetrates into the support structure. With increasing w_s the refractive index contrast between the optical grating and support structure decreases. As a result, the field is increasingly pulled into the support structure and the field in the upper region of the support structure increases. Figure 5 shows the elastic energy U_{elast} stored in one grating ridge for high-reflectivity configurations with different w_s. Here, we refer to the linear elastic energy density per unit length in the y-direction (compare Fig. 2):

$$U_{\mathrm{elast}} = \int \epsilon \mathrm{d}x\mathrm{d}z. \tag{16}$$

A frequency of 100 Hz was used. Figure 5 demonstrates that the ridge behaves like a loaded one-dimensional beam with

$$U_{\mathrm{elast}} = \frac{kx^2}{2} = \frac{F^2}{2k} \propto \frac{h_s}{w_s}. \tag{17}$$

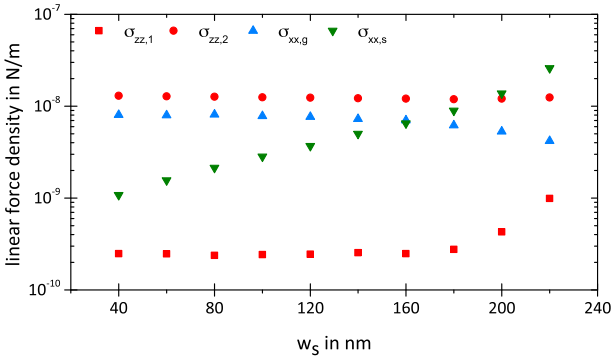

FIG. 4. Linear density of virtual forces (per unit length in the y-direction) at the surface.

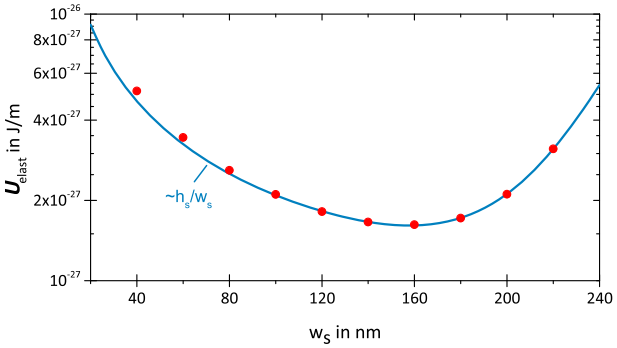

FIG. 5. Linear elastic energy density U_{elast} (per unit length in the y-direction) in dependence of the support grating width using a frequency of 100 Hz.

The ratio $\frac{w_s}{h_s}$ represents the spring constant k. For small w_s the elastic energy is dominated by the $1/w_s$ dependence. Reducing w_s the spring becomes softer and more elastic energy can be stored. For large w_s the thickness of the supporting structure needs to be increased to impede light from coupling to the substrate. The increased h_s again leads to a reduced spring constant and to higher elastic energies. The characteristic dependence on w_s is also evident in the thermal noise amplitude, which is shown in Fig. 6 for a frequency of 100 Hz and a temperature of 300 K. Thermal noise becomes minimal for a support structure width w_s of about 160 nm. At cryogenic temperatures Brownian thermal noise is further reduced due to decreased mechanical loss and temperature.

Deviations from the grating design parameters may not only influence the feasible reflectivity but also thermal noise. Therefore, we investigated thermal noise for possible parameter combinations obeying the reflectivity requirement of 99.99%. To this end, we utilized the parameters given in Table I as working points and performed an error

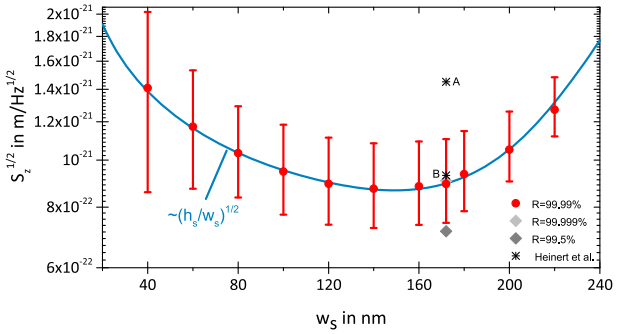

FIG. 6. Brownian noise amplitude at a frequency of 100 Hz, a temperature of 300 K, and a beam radius of 9 cm, resulting from the elastic energies shown in Fig. 5. In addition, data point A marks the calculation result by Heinert *et al.* [25]. For comparison, point B was calculated by applying Maxwell's stress tensor to the same grating parameters. The noise amplitudes for $R > 99.5\%$ and $R > 99.999\%$ are shown to illustrate the impact of the reflectivity requirement.

estimation by checking the dependence of thermal noise on the parameters h_s, w_s, h_g, and w_g. Thermal noise remains in the same order of magnitude for all relevant parameter combinations. Deviations of w_s change the spring constant of the grating and therefore make the largest contributions to changes in thermal noise. For small values of w_s the reflectivity requirement gives tolerances of about ± 10 nm, which are comparable to the values of w_s. That is why small values of w_s exhibit the error bars of maximum size.

Finally, we evaluate how thermal noise behaves for slightly different reflectivity requirements of $R > 99.5\%$ and $R > 99.999\%$. In both cases a w_s of 172 nm was chosen. Brownian thermal noise decreases by 20% for $R > 99.5\%$ and increases by 1.6% for $R > 99.999\%$. This variation of thermal noise is a consequence of reduced or enhanced h_s, which are necessary to achieve $R > 99.5\%$ and $R > 99.999\%$, respectively.

In comparison to the results by Heinert *et al.* [25] the calculation with Maxwell's stress tensor yields a thermal noise amplitude which is by a factor 0.61 smaller than the estimate given in the previous work (see Fig. 6). The complex field distribution utilized in the present article was treated as a homogenous averaged distribution in [25]. This leads to the observed deviations of the thermal noise amplitude. It should be noted that changes of the refractive index inside the dielectric material are neglected in the present study and may be subject to future work.

The electric field distribution and thus also the Brownian thermal noise of grating reflectors with 1D periodicity depend on the polarization of the incident light [see Eq. (13)]. Therefore, in the grating design the polarization dependence has to be carefully taken into account [35]. With advanced grating concepts such as 2D periodic structures this dependence can be overcome [20].

VI. CONCLUSION

We presented a method to calculate Brownian thermal noise in micro- and nanostructured surfaces. In our approach, computing the Maxwell stress tensor at the dielectric interface leads directly to the mechanical readout variable that is monitored by optical fields. The method is exact and computationally simpler compared to the approximate method developed by Heinert *et al.* [25], where the fluctuations of each structural part in all possible directions need to be considered separately to calculate the weighing factors. The application of the method to T-shaped monolithic grating reflectors reveals the following behavior: for small support widths, the elastic energy is high as the deformation of the support structure in response to the virtual forces becomes high. However, increasing the width requires a detrimental increase of the support structure depth in order to keep the reflectivity high. Therefore, for Brownian thermal noise an optimal w_s exists that all T-shaped grating designs should aim for. The presented method is applicable to arbitrary functional optical surface structures and incident light properties.

ACKNOWLEDGMENTS

The authors thank Frank Fuchs (Gitterwerk GmbH, Jena/Germany) for providing the RCWA code. S. K. acknowledges the support by the German Research Council (DFG) within research training group "NanoMet—Metrology for Complex Nanosystems" (GrK 1952/1). Y. L. acknowledges the support by the Australian Research Council Future Fellowship. S. P. V. acknowledges the support by the Russian Foundation for Basic Research (partially, Grant No. 16-52-10069); Russian Science Foundation (partially, Grant No. 17-12-01095); and National Science Foundation (partially, Grant No. PHY-130586). This document has LIGO No. P1700090.

[1] P. R. Saulson, Phys. Rev. D **42**, 2437 (1990).
[2] K. Numata, A. Kemery, and J. Camp, Phys. Rev. Lett. **93**, 250602 (2004).
[3] T. Kessler, C. Hagemann, C. Grebing, T. Legero, U. Sterr, F. Riehle, M. J. Martin, L. Chen, and J. Ye, Nat. Photonics **6**, 687 (2012).
[4] W. Zhang, M. Martin, C. Benko, J. L. Hall, J. Ye, C. Hagemann, T. Legero, U. Sterr, F. Riehle, G. D. Cole, and M. Aspelmeyer, Opt. Lett. **39**, 1980 (2014).
[5] C. Hagemann, C. Grebing, C. Lisdat, S. Falke, T. Legero, U. Sterr, F. Riehle, M. Martin, and J. Ye, Opt. Lett. **39**, 5102 (2014).
[6] S. Gras, H. Yu, W. Yam, D. Martynov, and M. Evans, Phys. Rev. D **95**, 022001 (2017).
[7] Y. Levin, Phys. Rev. D **57**, 659 (1998).
[8] G. M. Harry, A. Gretarsson, P. Saulson, S. E. Kittelberger, S. Penn, W. Startin, S. Rowan, M. M. Fejer, D. Crooks, G. Cagnoli, J. Hough, and N. Nakagawa, Classical Quantum Gravity **19**, 897 (2002).
[9] S. Penn, P. Sneddon, H. Armandula, J. Betzwieser, G. Cagnoli, J. Camp, D. Crooks, M. Fejer, and A. G. G. Harry, Classical Quantum Gravity **20**, 2917 (2003).
[10] S. Hild, M. Abernathy, F. Acernese *et al.*, Classical Quantum Gravity **28**, 094013 (2011).
[11] T. Hong, H. Yang, E. K. Gustafson, R. X. Adhikari, and Y. Chen, Phys. Rev. D **87**, 082001 (2013).
[12] G. Harry *et al.*, Classical Quantum Gravity **24**, 405 (2007).
[13] M. Principe, I. M. Pinto, V. Pierro, R. DeSalvo, I. Taurasi, A. E. Villar, E. D. Black, K. G. Libbrecht, C. Michel, N. Morgado, and L. Pinard, Phys. Rev. D **91**, 022005 (2015).

[14] G. Cole, W. Zhang, M. Martin, J. Ye, and M. Aspelmeyer, Nat. Photonics **7**, 644 (2013).
[15] A. V. Cumming, K. Craig, I. Martin, R. Bassiri, L. Cunningham, M. M. Fejer, J. Harris, K. Haughian, D. Heinert, B. Lantz, A. Lin, A. Markosyan, R. Nawrodt, R. Route, and S. Rowan, Classical Quantum Gravity **32**, 035002 (2015).
[16] A. Lin, R. Bassiri, S. Omar, A. S. Markosyan, B. Lantz, R. Route, R. L. Byer, J. S. Harris, and M. M. Fejer, Opt. Mater. Express **5**, 1890 (2015).
[17] M. Granata, E. Saracco, N. Morgado, A. Cajgfinger, G. Cagnoli, J. Degallaix, V. Dolique, D. Forest, J. Franc, C. Michel, L. Pinard, and R. Flaminio, Phys. Rev. D **93**, 012007 (2016).
[18] F. Brückner, T. Clausnitzer, O. Burmeister, D. Friedrich, E.-B. Kley, K. Danzmann, A. Tünnermann, and R. Schnabel, Opt. Lett. **33**, 264 (2008).
[19] F. Brückner, D. Friedrich, T. Clausnitzer, M. Britzger, O. Burmeister, K. Danzmann, E.-B. Kley, A. Tünnermann, and R. Schnabel, Phys. Rev. Lett. **104**, 163903 (2010).
[20] S. Kroker, T. Käsebier, S. Steiner, E.-B. Kley, and A. Tünnermann, Appl. Phys. Lett. **102**, 161111 (2013).
[21] S. Kroker, T. Käsebier, E.-B. Kley, and A. Tünnermann, Opt. Lett. **38**, 3336 (2013).
[22] P. Lalanne, J. Hugonin, and P. Chavel, J. Lightwave Technol. **24**, 2442 (2006).
[23] V. Karagodsky, F. Sedgwick, and C. Chang-Hasnain, Opt. Express **18**, 16973 (2010).
[24] H. Callen and T. A. Welton, Phys. Rev. **83**, 34 (1951).
[25] D. Heinert, S. Kroker, D. Friedrich, S. Hild, E.-B. Kley, S. Leavey, I. W. Martin, R. Nawrodt, A. Tünnermann, S. P. Vyatchanin, and K. Yamamoto, Phys. Rev. D **88**, 042001 (2013).
[26] M. G. Moharam and T. K. Gaylord, J. Opt. Soc. Am. **71**, 811 (1981).
[27] Y. Demchenko and M. L. Gorodetsky, Moscow Univ. Phys. Bull. **70**, 195 (2015).
[28] M. Tugolukov, Y. Levin, and S. Vyatchanin (to be published).
[29] https://www.comsol.com/multiphysics/finite-element method.
[30] V. Karagodsky and C. J. Chang-Hasnain, Opt. Express **20**, 10888 (2012).
[31] S. Kroker, E. B. Kley, and A. Tünnermann, Proc. SPIE **9372**, 93720F (2015).
[32] K. Yasumura, T. Stowe, E. Chow, T. Pfafman, T. Kenny, B. Stipe, and D. Rugar, J. Microelectromech. Syst. **9**, 117 (2000).
[33] H. Mamin and D. Rugar, Appl. Phys. Lett. **79**, 3358 (2001).
[34] J. Wortman and R. Evans, J. Appl. Phys. **36**, 153 (1965).
[35] J. Dickmann, C. B. R. Hurtado, R. Nawrodt, and S. Kroker (to be published).